A New Family of Streamline-Based Very High Resolution Schemes

F. Moukalled* and M. Darwish

American University of Beirut,
Faculty of Engineering & Architecture,
Mechanical Engineering Department,
P.O.Box: 11-0236
Beirut, Lebanon
email: memouk@aub.edu.lb

ABSTRACT

A number of High-Resolution (HR) schemes are reformulated in streamline-based coordinates and bounded using the Convection Boundedness Criterion (CBC) in the context of the Normalized Variable and Space Formulation methodology (NVSF). This new approach yields a family of Very High-Resolution (VHR) schemes that combines the advantages of the traditional HR schemes with the multi-dimensional nature of streamline-based schemes. The resultant VHR schemes, which are based on the MINMOD, OSHER, MUSCL, CLAM, SMART, STOIC, EXPONENTIAL, and SUPER-C HR schemes, are tested and compared with their base HR schemes by solving four problems: (i) pure convection of a step profile in an oblique velocity field; (ii) sudden expansion of an oblique velocity field in a rectangular cavity (iii) driven flow in a skew cavity; (iv) and gradual expansion in an axi-symmetric non-orthogonal channel. Results reveal that the new schemes are bounded and are by far more accurate than the original HR schemes in situations when the flow is highly skew to the grid lines.

* Author to whom all correspondence should be addressed

NOMENCLATURE

a	coefficient in the algebraic equation.
b	source term in the algebraic equation.
B	volume integral of source term Q.
C	convective flux.
e,w,n,s	east, west, north and south face of a control volume.
E,W,N,S	East, West, North and South neighbors of the P grid point.
f()	functional relationship.
J	total scalar flux across cell face.
P	dimensionless pressure; also main grid point.
p	thermodynamic pressure.
Q	Source term in the transport equation.
u, U	dimensional and dimensionless x-velocity.
v, V	dimensional and dimensionless y-velocity.
x, X	dimensional and dimensionless coordinate along the horizontal direction.
y, Y	dimensional and dimensionless coordinate along the vertical direction.

GREEK SYMBOLS

η	transformed coordinate.
μ	viscosity.
ξ	transformed coordinate.
ρ	density.
ϕ	dependent variable.
Γ	diffusion coefficient.

SUBSCRIPTS

C, D, U	Central, Downstream and Upstream grid points
dc	Deferred correction
e,w,n,s	east, west, north and south face of a control volume.
E,W,N,S	East, West, North and South neighbors of the P grid point.
f	Refers to any of the control volume faces.
nb	Refers to neighbors
P	refers to main grid point

SUPERSCRIPTS

'	correction value.
*	previous iteration value.
~	Refers to normalized variable.
C	Convection contribution.
D	Diffusion contribution.
U	Upwind formulation.

INTRODUCTION

When solving numerically fluid flow and heat transfer problems using a finite-difference or finite-volume method, results are seriously affected by the characteristics of the numerical scheme employed in calculating the convective flux, i.e. if accurate numerical solutions are to be obtained, the interpolation scheme used in calculating the advected quantities should be capable of reducing the errors arising from numerical diffusion in both the cross-stream and stream-wise directions. Cross-stream diffusion, as demonstrated by Raithby [1], Leschziner [2], and Patankar [3], occurs in a multi-dimensional flow when gradients in a convected quantity exist perpendicular to the flow and the direction of flow is oblique to the grid lines. On the other hand, stream-wise diffusion takes place when gradients in a convected quantity exist parallel to the flow [4] even in one-dimensional situations. In addressing the aforementioned issues, researchers have tried to improve the accuracy of numerical predictions by either reducing stream-wise diffusion through the use of higher-order schemes [5-7] or decreasing cross-stream diffusion by employing skew upwind schemes [8-11]. Both approaches yield more accurate schemes than the highly diffusive first order upwind scheme, however, these schemes suffer from a lack of boundedness, i.e. they tend to give rise to unphysical oscillations that induce large errors, known as numerical dispersion [12].

In tackling the emerging numerical dispersion problem, a variety of procedures have been advertised and may be divided into two major categories known as the flux-blending and flux-limiter techniques. The flux-blending approach may be decomposed into two classes. The first class is based on adding an anti-diffusive flux to a first-order upwind scheme [13] so as to resolve sharp gradients without undue under/over-shoots, while in the second class, some kind of smoothing diffusive agencies are introduced into an unbounded higher-order scheme [14-16] with the intention of damping oscillations. In general, due to their multi-step nature and the difficulty in balancing the two fluxes, accurate flux-blending techniques tend

to be very expensive computationally. The second approach, i.e. the flux-limiter method, is a cheaper way to remove unphysical oscillations. This technique is based on modifying the numerical flux at the interface of the computational cell by the use of a flux-limiter that enforces a monotonicity (boundedness) criterion. Higher-order schemes bounded by this approach are usually denoted by high-resolution (HR) schemes. The family of *"shock-capturing"* schemes based on the Total-Variation-Diminishing flux-limiters (TVD) [17], widely used in compressible flow simulations, are well known examples of this technique. A more recent formulation for high-resolution flux-limiters has been developed by Leonard [18] based on the Normalized Variable Formulation (NVF) methodology and generalized by Darwish and Moukalled [19] as the Normalized Variable and Space Formulation (NVSF) methodology.

A literature survey reveals that most unbounded higher-order schemes have been bounded through the use of one or more of the above methods [18,20-22]. On the contrary however, only few workers have implemented bounded streamline-based schemes. The unbounded skew upwind difference and the skew upwind weighted difference schemes were initially developed by Raithby [9]. Sharif and Busnaina [23] bounded the skew upwind difference scheme (SUDS) and the second-order upwind difference scheme (SOUDS) using two techniques. The first one is the Flux Corrected Transport (FCT) method developed by Boris and Book [24] and Book et al. [25] that was later improved by Zalesak [12]. The second technique is based on the Filtering Remedy and Methodology (FRAM) proposed by Chapman [14]. Sharif [11] has also used the FCT method to bound the directional transportive upwind differencing scheme (DTUDS). These bounding techniques follow the flux-blending approach and are thus expensive.

More recently, Darwish and Moukalled [26] advertised a new approach to bound skew schemes and applied it to the skew upwind scheme. The resulting NVF-SUDS [26] was applied to purely convective problems in Cartesian coordinates and its performance was

found to be impressive. However, for problems in which variations in the source term are important, the performance of the first order skew upwind scheme, on which the NVF-SUDS is based, degrades [9]. This degradation in performance is due to the importance of stream-wise diffusion which cannot be properly resolved by a first order interpolation profile. To reduce both components of diffusion, a streamline-based scheme of higher-order have to be used. This has lead Moukalled and Darwish [27] to consider the skew central difference scheme and to develop the NVF-SCDS which was shown to be by far more accurate then the NVF-SUDS in the above mentioned situations.

To this end, a similar approach as in [26,27] is adopted in this work and applied to a number of HR schemes developed using the TVD and NVSF methodologies to yield a new family of Very High-Resolution (VHR) schemes. This new technique is applied to the MINMOD [28] or SOUCOUP [29], OSHER [22] , MUSCL [21], CLAM [20], SMART [30], STOIC [31], EXPONENTIAL [32], and SUPER-C [33] schemes.

In what follows, the discretization procedure will first be presented along with a brief description of the NVSF methodology. Then the construction of the VHR schemes is detailed and the resultant VHR schemes tested and compared with the traditional HR schemes by solving four problems: (i) pure convection of a step profile in an oblique velocity field; (ii) sudden expansion of an oblique velocity field in a rectangular cavity (iii) driven flow in a skew cavity; (iv) and gradual expansion in an axi-symmetric non-orthogonal channel.

DISCRETIZATION OF THE TRANSPORT EQUATIONS

The transport equation governing two dimensional incompressible steady flows may be expressed in the following general form:

$$\vec{\nabla}.\left(\rho\vec{V}\phi\right) = \vec{\nabla}.\left(\Gamma\vec{\nabla}\phi\right) + Q \qquad (1)$$

where ϕ is any dependent variable, $\vec{V}$ is the velocity vector, and ρ, Γ, and Q are the density, diffusivity, and source terms respectively. Integrating the above equation over a control

volume, and applying the divergence theorem, the following discretized equation is obtained:

$$J_e + J_w + J_n + J_s = B \tag{2}$$

where J_f represent the total flux of ϕ across cell face 'f' (f= e, w, n or s) and is given by:

$$J_f = \left(\rho \vec{V}\phi - \Gamma^{\phi}\nabla\phi\right)_f . \vec{S}_f \tag{3}$$

and B is the volume integral of the source term Q. Each of the surface fluxes J_f contains a convective contribution, J_f^C , and a diffusive contribution, J_f^D , hence:

$$J_f = J_f^C + J_f^D \tag{4}$$

where

$$J_f^C = \left(\rho \vec{V}\phi\right)_f . \vec{S}_f \qquad J_f^D = \left(-\Gamma^{\phi}\nabla\phi\right)_f . \vec{S}_f \tag{5}$$

The diffusive flux at the control volume face 'f' is discretized using a linear symmetric interpolation profile so as to write the gradient as a function of the neighboring grid points. The discretization of the convective flux however requires estimating the value of the dependent variable along the control volume face from the values at the main grid points. Depending on the interpolation profile employed, a functional relationship of the following form is generally obtained:

$$\phi_f = f(\phi_{nb}) \tag{6}$$

where the subscript nb designates neighboring grid points. Substituting the discretized forms of the diffusive and convective fluxes into Eq. (2) and performing some algebraic manipulations, the discretized form of Eq. (1) becomes:

$$a_P \phi_P = \sum_{nb}\left(a_{nb}\phi_{nb}\right) + b_P \tag{7}$$

where the coefficients a_P and a_{nb} depend on the selected scheme and b_P is the source term of the discretized equation.

Since the functional relationship can involve a large number of neighboring grid points, especially when using HR or Streamline-based schemes, the solution of Eq. (7) can become

very expensive computationally, hence the need for a compacting procedure. In the present work the deferred correction procedure of Rubin and Khosla [34] is used. In this procedure Eq. (2) is rewritten as:

$$J_e^U + J_w^U + J_n^U + J_s^U = B + \underline{\left[C_e(\phi_e^U - \phi_e) - C_w(\phi_w^U - \phi_w) + C_n(\phi_n^U - \phi_n) - C_s(\phi_s^U - \phi_s)\right]} \quad (8)$$

where ϕ_f^U is the face value calculated using the first order upwind scheme, J_f^U the total flux of ϕ, with the convective part calculated using the first order upwind scheme, ϕ_f the cell face value calculated using the chosen streamline-based or high-resolution scheme, and the underlined terms represent the extra source term due to the deferred correction. Substituting the value of the cell flux obtained from the functional relationship of the upwind and HR or skew scheme at hand, the deferred correction results in an equation similar in form to Eq. (7), but where the coefficient matrix is penta-diagonal (for 2D) and always diagonally dominant since it is formed using the first order upwind scheme. The discretized equation, Eq. (8), becomes:

$$a_P \phi_P = \sum_{nb}\left(a_{nb}\phi_{nb}\right) + b_P + b_{dc} \quad (9)$$

where now the coefficients a_P and a_{nb} are obtained from a first order upwind discretization, nb=(E,W,S,N), and b_{dc} is the extra deferred correction source term. This compacting procedure is simple to implement and effective when using streamline-based or high-resolution schemes.

To calculate the pressure field that arise in the simulation of fluid flows the SIMPLE algorithm of Patankar [3] along with collocated variables and a special interpolation practice for the calculation of the mass fluxes across the control volume faces developed by Peric [15] are used. Since the paper focuses on the construction of a new family of VHR schemes, details regarding the solution procedure are not given and readers are referred to Rodi [35] for further information.

THE NVSF METHODOLOGY FOR CONSTRUCTING HR SCHEMES

Before introducing the VHR streamline-based schemes a brief review of the NVSF methodology is in order. First the Normalized Variable is presented along with the Convection Boundedness Criterion (CBC), then the MINMOD, OSHER, MUSCL, CLAM, SMART, STOIC, EXPONENTIAL, and SUPER-C HR schemes are described. These schemes will be used in constructing a family of VHR schemes

NORMALIZED VARIABLES

Fig.1(a) shows the local behavior of the convected variable near a control-volume face. The node labeling refers to the upstream, central, and downstream grid points designated by U, C, and D, located at distances ξ_U, ξ_C and ξ_D from the origin, respectively. The values of ϕ at these nodes are designated by ϕ_U, ϕ_C and ϕ_D respectively. Moreover, the value of the dependent variable at the control volume face located at a distance ξ_f from the origin is expressed by ϕ_f. Since a normalized variable and space formulation is sought, the following normalized variables are defined:

$$\tilde{\phi} = \frac{\phi - \phi_U}{\phi_D - \phi_U} \qquad \tilde{\xi} = \frac{\xi - \xi_U}{\xi_D - \xi_U} \tag{10}$$

Using $\tilde{\phi}_f$, the boundedness requirements can be easily formulated.

THE CONVECTIVE BOUNDEDNESS CRITERION (CBC)

Based on the normalized variable analysis, Gaskell and Lau [30] formulated a convection boundedness criterion (CBC) for implicit steady flow calculation, which states that for a scheme to have the boundedness property its functional relationship should be continuous, should be bounded from below by $\tilde{\phi}_f = \tilde{\phi}_C$, from above by unity, and should pass through the points (0,0) and (1,1), in the monotonic range ($0< \tilde{\phi}_C <1$), and for $1<\tilde{\phi}_C$ or $\tilde{\phi}_C <0$, the

functional relationship f($\tilde{\phi}_C$) should equal $\tilde{\phi}_C$. The above conditions may also be illustrated on a Normalized Variable Diagram (NVD) as shown in Fig. 1(b).

NORMALIZED VARIABLE AND SPACE FORMULATION (NVSF) METHODOLOGY

Knowing the required conditions for boundedness, the shortcomings of the HO schemes were eliminated through the development of HR schemes satisfying all above requirements. Without going into details, a number of HR schemes were formulated using the NVSF methodology and the functional relationships for some of them is given below. For more details the reader is referred to Darwish and Moukalled [19].

MINMOD or SOUCOUP

$$\tilde{\phi}_f = \begin{cases} \dfrac{\tilde{\xi}_f}{\tilde{\xi}_C}\tilde{\phi}_C & 0 < \tilde{\phi}_C < \tilde{\xi}_C \\ \dfrac{1-\tilde{\xi}_f}{1-\tilde{\xi}_C}\tilde{\phi}_C + \dfrac{\tilde{\xi}_f - \tilde{\xi}_C}{1-\tilde{\xi}_C} & \tilde{\xi}_C \le \tilde{\phi}_C < 1 \\ \tilde{\phi}_C & \text{elsewhere} \end{cases} \tag{11}$$

OSHER

$$\tilde{\phi}_f = \begin{cases} \dfrac{\tilde{\xi}_f}{\tilde{\xi}_C}\tilde{\phi}_C & 0 < \tilde{\phi}_C < \dfrac{\tilde{\xi}_C}{\tilde{\xi}_f} \\ 1 & \dfrac{\tilde{\xi}_C}{\tilde{\xi}_f} \le \tilde{\phi}_C < 1 \\ \tilde{\phi}_C & \text{elsewhere} \end{cases} \tag{12}$$

EXPONENTIAL

$$\tilde{\phi}_f = \begin{cases} 1.125\left(1 - e^{-2.19722\tilde{\phi}_C}\right) & 0 < \tilde{\phi}_C < 1 \\ \tilde{\phi}_C & \text{elsewhere} \end{cases} \tag{13}$$

MUSCL

$$\tilde{\phi}_f = \begin{cases} \dfrac{2\tilde{\xi}_f - \tilde{\xi}_C}{\tilde{\xi}_C}\tilde{\phi}_C & 0 < \tilde{\phi}_C < \dfrac{\tilde{\xi}_C}{2} \\ \tilde{\phi}_C + \left(\tilde{\xi}_f - \tilde{\xi}_C\right) & \dfrac{\tilde{\xi}_C}{2} \le \tilde{\phi}_C < 1 + \tilde{\xi}_C - \tilde{\xi}_f \\ 1 & 1 + \tilde{\xi}_C - \tilde{\xi}_f \le \tilde{\phi}_C < 1 \\ \tilde{\phi}_C & \text{elsewhere} \end{cases} \tag{14}$$

CLAM

$$\tilde{\phi}_f = \begin{cases} \dfrac{\left(\tilde{\xi}_C{}^2 - \tilde{\xi}_f\right)}{\tilde{\xi}_C\left(\tilde{\xi}_C - 1\right)}\tilde{\xi}_C + \dfrac{\left(\tilde{\xi}_f - \tilde{\xi}_C\right)}{\tilde{\xi}_C\left(\tilde{\xi}_C - 1\right)}\tilde{\xi}_C{}^2 & 0 < \tilde{\phi}_C < 1 \\ \tilde{\phi}_C & \text{elsewhere} \end{cases} \tag{15}$$

SMART

$$\tilde{\phi}_f = \begin{cases} \dfrac{\tilde{\xi}_f\left(1 - 3\tilde{\xi}_C + 2\tilde{\xi}_f\right)}{\tilde{\xi}_C\left(1 - \tilde{\xi}_C\right)}\tilde{\phi}_C & 0 < \tilde{\phi}_C < \dfrac{\tilde{\xi}_C}{3} \\ \dfrac{\tilde{\xi}_f\left(1 - \tilde{\xi}_f\right)}{\tilde{\xi}_C\left(1 - \tilde{\xi}_C\right)}\tilde{\phi}_C + \dfrac{\tilde{\xi}_f\left(\tilde{\xi}_f - \tilde{\xi}_C\right)}{1 - \tilde{\xi}_C} & \dfrac{\tilde{\xi}_C}{3} \le \tilde{\phi}_C < \dfrac{\tilde{\xi}_C}{\tilde{\xi}_f}\left(1 + \tilde{\xi}_f - \tilde{\xi}_C\right) \\ 1 & \dfrac{\tilde{\xi}_C}{\tilde{\xi}_f}\left(1 + \tilde{\xi}_f - \tilde{\xi}_C\right) \le \tilde{\phi}_C < 1 \\ \tilde{\phi}_C & \text{elsewhere} \end{cases} \tag{16}$$

STOIC

$$\tilde{\phi}_f = \begin{cases} \dfrac{\tilde{\xi}_f\left(1 - 3\tilde{\xi}_C + 2\tilde{\xi}_f\right)}{\tilde{\xi}_C\left(1 - \tilde{\xi}_C\right)}\tilde{\phi}_C & 0 < \tilde{\phi}_C < \dfrac{\tilde{\xi}_C\left(\tilde{\xi}_C - \tilde{\xi}_f\right)}{\tilde{\xi}_C + \tilde{\xi}_f + 2\tilde{\xi}_f^2 - 4\tilde{\xi}_f\tilde{\xi}_C} \\ \dfrac{1 - \tilde{\xi}_f}{1 - \tilde{\xi}_C}\tilde{\phi}_C + \dfrac{\tilde{\xi}_f - \tilde{\xi}_C}{1 - \tilde{\xi}_C} & \dfrac{\tilde{\xi}_C\left(\tilde{\xi}_C - \tilde{\xi}_f\right)}{\tilde{\xi}_C + \tilde{\xi}_f + 2\tilde{\xi}_f^2 - 4\tilde{\xi}_f\tilde{\xi}_C} \le \tilde{\phi}_C < \tilde{\xi}_C \\ \dfrac{\tilde{\xi}_f\left(1 - \tilde{\xi}_f\right)}{\tilde{\xi}_C\left(1 - \tilde{\xi}_C\right)}\tilde{\phi}_C + \dfrac{\tilde{\xi}_f\left(\tilde{\xi}_f - \tilde{\xi}_C\right)}{1 - \tilde{\xi}_C} & \tilde{\xi}_C \le \tilde{\phi}_C < \dfrac{\tilde{\xi}_C}{\tilde{\xi}_f}\left(1 + \tilde{\xi}_f - \tilde{\xi}_C\right) \\ 1 & \dfrac{\tilde{\xi}_C}{\tilde{\xi}_f}\left(1 + \tilde{\xi}_f - \tilde{\xi}_C\right) < \tilde{\phi}_C < 1 \\ \tilde{\phi}_C & \text{elsewhere} \end{cases} \tag{17}$$

SUPER-C

$$\tilde{\phi}_f = \begin{cases} \dfrac{\tilde{\xi}_f\left(1-3\tilde{\xi}_C+2\tilde{\xi}_f\right)}{\tilde{\xi}_C\left(1-\tilde{\xi}_C\right)}\tilde{\phi}_C & 0<\tilde{\phi}_C<\dfrac{2}{5}\tilde{\xi}_C \\ \dfrac{1-\tilde{\xi}_f}{1-\tilde{\xi}_C}\tilde{\phi}_C+\dfrac{\tilde{\xi}_f-\tilde{\xi}_C}{1-\tilde{\xi}_C} & \dfrac{2}{5}\tilde{\xi}_C\le\tilde{\phi}_C<\tilde{\xi}_C \\ \dfrac{\tilde{\xi}_f\left(1-\tilde{\xi}_f\right)}{\tilde{\xi}_C\left(1-\tilde{\xi}_C\right)}\tilde{\phi}_C+\dfrac{\tilde{\xi}_f\left(\tilde{\xi}_f-\tilde{\xi}_C\right)}{1-\tilde{\xi}_C} & \tilde{\xi}_C\le\tilde{\phi}_C<\dfrac{\tilde{\xi}_C}{\tilde{\xi}_f}\left(1+\tilde{\xi}_f-\tilde{\xi}_C\right) \\ 1 & \dfrac{\tilde{\xi}_C}{\tilde{\xi}_f}\left(1+\tilde{\xi}_f-\tilde{\xi}_C\right)<\tilde{\phi}_C<1 \\ \tilde{\phi}_C & \text{elsewhere} \end{cases} \tag{18}$$

STREAMLINE-BASED INTERPOLATION

In order to be able to apply the various HR schemes in streamline-based coordinates, ϕ estimates at three locations (two upstream and one downstream) in the direction of the local velocity vector are needed. For that purpose, the direction of the velocity vector at the cell face is considered to determine the streamline direction and interpolation is carried among the appropriate nodes surrounding the cell face to obtain the Upstream ($\underline{\phi}_U$), Central ($\underline{\phi}_C$), and Downstream ($\underline{\phi}_D$) nodal values in the skew direction (Fig. 1(c)). For the configuration shown in Fig. 1(c), these estimates are given by:

$$\begin{aligned} \underline{\phi}_U &= m_1\phi_{SW}+m_2\phi_{SSW} \\ \underline{\phi}_C &= m_3\phi_P+m_4\phi_S \\ \underline{\phi}_D &= m_5\phi_{NE}+m_6\phi_E \end{aligned} \tag{19}$$

where m_1, m_2, m_3, m_4, m_5, and m_6 are weighing factors that depend on geometrical quantities. Definitely, higher interpolation profiles may be used which may give better results. However, for the results generated in this paper, the use of the linear interpolation profile was found to be adequate.

Using these interpolated estimates the interface value is calculated employing expressions

similar to those of the HR schemes. However the local coordinate system used is no more the mesh coordinate system, but rather, the streamline coordinate system. Thus the spatial distances are now calculated along the streamline direction.

Having obtained the necessary values in the streamline direction, the next step is to be able to apply the functional relationships of HR schemes along that direction in a bounded manner (i.e. without undue under/over shoots). Thus the following normalized variables are used in place of those defined in Eq. (10).

$$\underline{\tilde{\phi}} = \frac{\phi - \underline{\phi}_U}{\underline{\phi}_D - \underline{\phi}_U} \qquad \underline{\tilde{\xi}} = \frac{\xi - \underline{\xi}_U}{\underline{\xi}_D - \underline{\xi}_U} \tag{20}$$

BOUNDING STRATEGY

When calculating ϕ_f using the original HR schemes, the Upstream, Central, and Downstream **nodal** values are available and need not be interpolated. In streamline-based coordinates, however, estimates at these locations, as mentioned earlier, are not available and should be obtained by interpolation. Since a linear interpolation profile is used, the resulting control volume face value may not always be bounded in the physical sense (i.e. even though the CBC is enforced along the streamline direction the calculated face value can still be outside the range set by the two points neighboring the face). To further clarify, the calculated face value is bounded with respect to the interpolated skew values ($\underline{\phi}_U$, $\underline{\phi}_C$, $\underline{\phi}_D$) but not necessarily with respect to the ϕ values at the centers of the control volumes surrounding the face (ϕ_U, ϕ_C, ϕ_D). In order to eliminate any unphysical results, after the calculation of $\tilde{\phi}_f$ using any of the above schemes, the face value is de-normalized to yield ϕ_f and then the CBC is enforced using the appropriate **nodal** values (ϕ_U, ϕ_C, and ϕ_D (Fig. 1(a))) in the event when it is not satisfied. Results obtained using this technique (designated here by METHOD 1) were properly bounded, while results obtained without applying the second bounding procedure

(denoted here by METHOD 2) showed undue oscillations which justifies the need to perform the second bounding step.

RESULTS AND DISCUSSION

To check the performance of the new VHR schemes against their traditional HR counterparts, one purely convective problem and three flow problems are solved. Results are obtained by covering the physical domains with uniform grids. Grid networks are generated using the Transfinite interpolation technique [36]. In all tests, computational results are considered converged when the residual error (RE) defined as:

$$RE = \underset{i=1}{\overset{n}{MAX}}\left[\left| a_P\phi_P - \left(\sum_{NB} a_{NB}\phi_{NB} + b_P + b_{dc}\right)\right|\right] \tag{21}$$

became smaller than a vanishing quantity.

Before presenting and discussing results, it should be made clear that the objective of the paper is to develop and test a new family of skew VHR schemes. Since the new family is streamline-based, it is natural to choose the flow in some of the test problems to be skewed to the grid lines. Moreover, the comparison between the HR and VHR schemes is made for the sole purpose of showing that for the same number of grid points the VHR schemes are more accurate than the respective HR schemes.

TEST 1: PURE CONVECTION OF A STEP PROFILE IN AN OBLIQUE VELOCITY FIELD

Figure 2 shows the well known benchmark test problem consisting of a pure convection of a transverse step profile imposed at the inflow boundaries of a square computational domain. A 27x27 mesh is used giving $\Delta x = \Delta y = 1/25$. The angle θ is chosen to be 45° and $|\mathbf{V}| = 1$. The governing conservation equation of the problem is:

$$\frac{\partial(U\phi)}{\partial X} + \frac{\partial(V\phi)}{\partial Y} = 0 \tag{22}$$

where ϕ is the dependent variable and U and V are the Cartesian components of the uniform velocity vector $\vec{V}$. The computed values of ϕ using the various HR schemes, VHR schemes, and the exact analytical solution to the problem are shown, along the vertical centerline of the domain, in Figs. (3) and (4). The displayed VHR schemes' profiles are obtained by METHOD 1. For this problem, where gradients are important, METHOD 2 resulted in unphysical oscillations for the reasons stated earlier. The results presented are very clear and self explanatory. The best results obtained are for the VHR schemes (METHOD 1) which are very accurate and oscillations free since the CBC is enforced. The performance of all VHR schemes is similar in this problem, due to the fact that, in the streamline direction, ϕ is constant. The estimates generated by the HR schemes, as revealed by the displayed profiles, are of quality lower than those obtained with the skew schemes due to the high importance of cross-stream diffusion.

TEST 2: SUDDEN EXPANSION OF AN OBLIQUE FLOW FIELD IN A RECTANGULAR CAVITY

The physical situation under consideration is depicted in Fig. 5. The flow is assumed to be steady, laminar, and two-dimensional. The non-dimensional mass, and momentum equations governing the flow field are:

$$\frac{\partial U}{\partial X}+\frac{\partial V}{\partial Y}=0 \tag{23}$$

$$U\frac{\partial U}{\partial X}+V\frac{\partial U}{\partial Y}=-\frac{\partial P}{\partial X}+\frac{1}{Re}\left[\frac{\partial^2 U}{\partial X^2}+\frac{\partial^2 U}{\partial Y^2}\right] \tag{24}$$

$$U\frac{\partial V}{\partial X}+V\frac{\partial V}{\partial Y}=-\frac{\partial P}{\partial Y}+\frac{1}{Re}\left[\frac{\partial^2 V}{\partial X^2}+\frac{\partial^2 V}{\partial Y^2}\right] \tag{25}$$

where the following dimensionless variables have been defined:

$$X=\frac{x}{L}, Y=\frac{y}{L}\quad U=\frac{u}{V_{ref}}, V=\frac{v}{V_{ref}}\quad P=\frac{p}{\rho V_{ref}^2} \tag{26}$$

The boundary conditions used are:

$$U = 1 \qquad V = 1 \qquad \text{at} \qquad \text{inlet} \tag{27}$$

$$\frac{\partial U}{\partial X} = \frac{\partial V}{\partial X} = 0 \qquad \text{at} \qquad \text{exit} \tag{28}$$

$$U = V = 0 \qquad \text{elsewhere} \tag{29}$$

The problem is solved using the following HR and VHR schemes: MINMOD, CLAM, SMART, and STOIC for a value of Reynolds number ($Re=\rho V_{ref}L/\mu$, L the cavity height or width and V_{ref} the reference velocity) of 500. The U- and V-velocity components along the vertical and horizontal centerlines of the domain are presented in Figs. 6 and 7 respectively. In these figures, the profiles generated by the various HR and VHR schemes (METHOD 1 and METHOD 2) employing 22x22 grid points are compared against the profile obtained using the SMART scheme with a dense grid of size 42x42. The profiles generated by METHOD 2 show some unboundedness and are not accurate. Results generated by METHOD 1, however, are bounded and very accurate.

As depicted, great improvements are achieved with all schemes. However, the rate of improvement is higher for the second order MINMOD and CLAM schemes (Figs. 6(a), 6(b), 7(a), and 7(b)) which are more diffusive than the other HR schemes. With all schemes, the profiles generated are almost as accurate as the one generated by SMART using the dense grid. This improvement in results is due to the importance of cross-stream diffusion which is easily resolved by the skew schemes.

This problem has clearly demonstrated the importance of resolving cross-stream diffusion and has shown that skew interpolation profiles are by far better than one-dimensional interpolation profiles when the flow field is skew with respect to the grid lines.

TEST 3: DRIVEN FLOW IN A SKEW CAVITY

A schematic of the physical situation and streamlines are depicted in Fig. 8. The governing equations of the problem are the same as for the previous one (Eqs. (25)-(27)). However, the dimensionless parameters are defined as:

$$X = \frac{x}{L}, Y = \frac{y}{L} \quad U = \frac{u}{u_s}, V = \frac{v}{u_s} \quad P = \frac{p}{\rho u_s^2} \tag{30}$$

and the applicable boundary conditions are:

$$U = 1 \qquad V = 0 \qquad \text{at} \qquad Y = 1 \tag{31}$$

$$U = V = 0 \qquad \text{elsewhere} \tag{32}$$

Results are presented for a value of Reynolds number ($Re=\rho u_s L/\mu$, L the cavity height or width and u_s the velocity of the top horizontal wall) of 500. The side walls are skewed at an angle of 45° with respect to the horizontal. The problem is solved using the various schemes and a number of grid sizes. The U-velocity profiles at X=0.85 generated by the HR and VHR schemes using 22x22 grid points are compared, in Figs. 9 and 10, against the profile predicted by SMART using a grid size of 62x62.

Improvements in results are obtained with all skew schemes with its degree varying with the scheme. Even though results obtained with METHOD 2 are, for some of the schemes, better than those obtained by METHOD 1, in general, profiles do not lie between those generated by the HR schemes using 22x22 grid points and the SMART scheme using 62x62 grid points (see. e.g. Figs. 10(a), 10(b), and 10(d)). This is an indication of the instability of METHOD 2. On the contrary, however, results generated by METHOD 1 are very stable and always lie between those generated by the respective HR scheme using a coarse grid and the SMART scheme using the dense grid.

This problem has demonstrated once more that the use of skew schemes reduces cross-stream diffusion and improve the solution accuracy.

TEST 4: GRADUAL EXPANSION IN AN AXI-SYMMETRIC NON-ORTHOGONAL CHANNEL

The last problem presented deals with a gradual expansion of a fluid in a non-orthogonal axisymmetric geometry. A schematic of the physical situation, the computed flow field, the channel's dimensions, and the equation used to generate the channel's surface are depicted in Fig. 11(a). The conservation of mass and momentum equations governing the flow field are given by:

$$\frac{\partial U}{\partial X}+\frac{1}{R}\frac{\partial}{\partial R}(RV)=0 \tag{33}$$

$$\frac{\partial}{\partial X}\left(U^2\right)+\frac{1}{R}\frac{\partial}{\partial R}(RUV)=-\frac{\partial P}{\partial X}+\frac{1}{Re}\frac{\partial}{\partial X}\left(\frac{\partial U}{\partial X}\right)+\frac{1}{Re}\frac{1}{R}\frac{\partial}{\partial R}\left(R\frac{\partial U}{\partial R}\right) \tag{34}$$

$$\frac{\partial}{\partial X}(UV)+\frac{1}{R}\frac{\partial}{\partial R}\left(RV^2\right)=-\frac{\partial P}{\partial R}+\frac{1}{Re}\frac{\partial}{\partial X}\left(\frac{\partial V}{\partial X}\right)+\frac{1}{Re}\frac{1}{R}\frac{\partial}{\partial R}\left(R\frac{\partial V}{\partial R}\right)-\frac{1}{Re}\frac{V}{R^2} \tag{35}$$

where the following dimensionless variables have been used:

$$U=\frac{u}{u_{in}},V=\frac{v}{u_{in}},R=\frac{r}{r_i},X=\frac{x}{r_i},P=\frac{p}{\rho u_{in}^2} \tag{36}$$

The boundary conditions employed are:

$$U=1 \qquad V=0 \qquad \text{at} \qquad \text{inlet} \tag{37}$$

$$U=V=0 \qquad \text{along} \quad \text{walls} \tag{38}$$

$$\frac{\partial U}{\partial X}=\frac{\partial V}{\partial X}=0 \qquad \text{at} \quad \text{exit} \tag{39}$$

The problem is solved for a Reynolds number ($Re=\rho u_{in} r_i/\mu$, where $r_i=1$) of 100. The length L of the pipe (=Re/6) is long enough to safely apply the outflow boundary condition. The U-velocity profiles at X=6, generated using the MINMOD and SMART schemes, are displayed in Figs. 11(b) and 11(c), respectively. As shown, the performance of the multi-dimensional MINMOD scheme is much better than the performance of its one-dimensional counterpart. However, the profile generated by the skew SMART scheme is comparable (slightly better) to that generated by the third-order one-dimensional SMART scheme. This slight difference in results between SMART and skew SMART is due to the low value of cross-stream

diffusion, which is better resolved by the SMART scheme but not the MINMOD scheme, and the alignment, more or less, of the flow with the grid lines. This behavior is anticipated and the problem is deliberately chosen to clearly demonstrate that when stream-wise diffusion is dominant and the skewness of the flow with respect to the grid lines is low, the performance of the VHR schemes is similar to that of the HR schemes. Since the VHR schemes are relatively more expensive than the HR schemes, it is computationally more economical to use them only when needed. Thus, the best framework for implementing these VHR schemes is through an adaptive strategy, whereby a criterion, dependent on the flow skewness, is used for switching between a HR and a VHR scheme. This research topic is currently being addressed by the authors.

CONCLUDING REMARKS

A new family of very high resolution (VHR) scheme was developed. The new schemes are extensions of the well known HR schemes into streamline-based coordinates. The newly developed VHR schemes are bounded using the CBC and their performance is tested in Cartesian, planar curvilinear, and axisymmetric non-orthogonal curvilinear coordinates by solving four problems. By comparing the performance of the new skew schemes against their pseudo one-dimensional forms, it can be safely stated that the best performance can always be obtained with high-order skew schemes. Two issues that should be further investigated are the implementation of such schemes through an adaptive strategy and the performance of these schemes in three-dimensional spaces.

ACKNOWLEDGMENTS

The financial support provided by the University Research Board of the American University of Beirut through grant No. 48020 is gratefully acknowledged.

REFERENCES

1. Raithby, G.D., “A Critical Evaluation of Upstream Differencing Applied to Problems Involving Fluid Flow,” Comp. Methods Applied Mech. & Eng., vol. 9, pp. 75-103, 1976.

2. Leschziner, M.A.,“Practical Evaluation of Three Finite Difference Schemes for the Computation of Steady-State Recirculating Flows,” Comput. Methods Appl. Mech. Eng., vol. 23, pp. 293-311, 1980.

3. Patankar, S.V., Numerical Heat Transfer and Fluid Flow, Hemisphere Publishing Corporation, 1981.

4. Runchal, A. K., “Condif: A Modified Central-Difference Scheme for Convective Flows,” Int. J. Num. Methods Eng., vol. 24, pp. 1593-1608, 1987.

5. Leonard, B.P., “A Stable and Accurate Convective Modelling Procedure Based on Quadratic Interpolation, Comp. Methods. Applied Mech. & Eng., vol. 19, pp. 59-98, 1979.

6. Leonard, B.P., “A Survey of Finite Differences with Upwinding for Numerical Modelling of the Incompressible Convective Diffusion Equation,” in Computational Techniques in Transient and Turbulent Flow, vol. 2, eds.: Taylor C., Morgan K., Pub. Pineridge Press Ltd, 1981.

7. Agarwal, R.K.,“A Third Order Accurate Upwind Scheme for Navier Stokes solutions in Three Dimensions,” in K.N. Ghia T.J. Mueller B.R. Patel (eds): Computers in flow prediction and fluid dynamics experiments. ASME winter meeting, Washington, pp. 73-82, 1981.

8. Fromm, J.E., “A Method for reducing dispersion in Convective Difference Schemes,” Comput. Phys., vol. 3, pp. 176-189, 1986.

9. Raithby, G.D., “Skew Upstream Differencing Schemes for Porblems Involving FLuid Flow,” J. of Comp. Methods Appl. Mech. & Eng., vol. 9, pp. 153-164, 1976.

10. Lilington, J.N., “A Vector Upstream Differencing Scheme for Problems in Fluid Flow Involving Significant Source Terms in Steady-State Linear Systems,” Int. J. Num. Methods Fluids, vol. 1, pp. 3-16, 1981.

11. Sharif, M.A.R., “An evaluation of the Bounded Directional Transportive Upwind Differencing Scheme for the Convection-Diffusion Problems,” Num. Heat Transfer, vol. 23, pp. 201-219, 1993.

12. Hassan, Y.A., Rice, J.G., and Kin, J.H., “A Stable Mass-Flow-Weighted Two-Dimensional Skew Upwing Scheme,” Num. Heat Trasfer, vol. 6, pp. 395-408, 1983.

13. Zalesak, S.T., “Fully Multidimensional Flux-Corrected Transport Algorithms for Fluids,” J. Comp. Phys., vol. 31, pp. 335-362, 1979.

14. Chapman, M., “FRAM Nonlinear Damping Algorithm for the Continuity Equation,” J. Comp. Phys., vol 44, pp. 84-103, 1981.

15. Peric, M., A Finite Volume Method for the Prediction of Three Dimensional Fluid Flow in Complex Ducts, Ph.D. Thesis, Imperial College, Mechanical Engineering Department, 1985.

16. Zhu, J. and Leschziner, M.A., “A Local Oscillation-Damping Algorithm for Higher Order Convection Schemes,” Comp. Methods Appl. Mech. & Eng., vol. 67, pp. 355-366, 1988.

17. Sweby, P. K., “High Resolution Schemes Using Flux Limiters for Hyperbolic Conservation Laws,” SIAM J. Num. Anal., vol. 21, pp. 995-1011, 1984.

18. Leonard, B. P., “Simple High-Accuracy Resolution Program for Convective Modelling of Discontinuities,” Int. J. Num. Meth. Eng., vol 8, pp. 1291-1318, 1988.

19. Darwish, M. and Moukalled, F.,"Normalized Variable and Space Formulation Methodology for High-Resolution Schemes," Numerical Heat Transfer, Part B, vol. 26, No. 1, pp. 79-96, 1994.

20. Van Leer, B., “Towards the Ultimate Conservative Difference Scheme. II. Monotonicity and Conservation Combined in a Second Order Scheme,” J. Comput. Phys., vol. 14, pp. 361-370, 1974.

21. Van Leer, B., “Towards the Ultimate Conservative Difference Scheme. V. A Second-Order Sequel to Godunov's Method,” J. Comput. Phys., vol. 23, pp. 101-136, 1977.

22. Chakravarthy, S. R. and Osher, S., “High Resolution Applications of the OSHER Upwind Scheme for the Euler Equations,” AIAA Paper 83-1943, 1983.

23. Sharif, M.A.R. and Busnaina, A.A., “Evaluation and Comparison of Bounding techniques for Convection-Diffusion Problems,” J. Fluid Eng., vol 115, pp. 33-40, 1983.

24. Boris, J.P.,and Book, D.L.,”Flux-Corrected Transport. I. SHASTA, A fluid Transport Algorithm that Works,” J. Comp. Phys., vol 11, pp. 38-69, 1973.

25. Book, D.L., Boris, J.P., and Hain, K.,”Flux-Corrected Tranport II: Generalizations of the Method,” J. Comp. Phys., vol 18, pp. 248-283, 1975.

26. Darwish, M., and Moukalled, F., "A New Approach for Building Skew-Upwind Schemes," Comput. Methods Appl. Mech. Engrg., vol. 129, pp. 221-233, 1996.

27. Moukalled, F. and Darwish, M.,” A New Bounded Skew Central Difference Scheme, Part I. Formulation and Testing,” Numerical Heat Transfer, Part B, Vol. 31, No. 1, pp. 111-133, 1997.

28. Harten, A., “High Resolution Schemes for Hyperbolic Conservation Laws,” J. Comput. Phys., vol. 49, pp. 357-393, 1983.

29. Zhu, J. And Rodi, W., “A Low Dispersion and Bounded Convection Scheme,” Comp. Methods Appl. Mech. & Eng., vol. 92, pp. 87-96, 1991.

30. Gaskell, P.H. and Lau, A.K.C., “Curvature Compensated Convective Transport: SMART, a New Boundedness Preserving Transport Algorithm,” Int. J. Num. Meth. Fluids, vol. 8, pp. 617-641, 1988.

31. Darwish, M.S., ”A New High Resolution Scheme Based on the Normalized Variable Formulation,” Numerical Heat Transfer, Part B, vol. 24, pp. 353-371, 1993.

32. Leonard, B. P., “Locally Modified Quick Sheme for Highly Convective 2-D and 3-D Flows,” C. Taylor and K. Morgan (eds.), Numerical Methods in Laminar and Turbulent Flows, Pineridge Press, Swansea, U.K., vol. 5, pp. 35-47, 1987.

33. Leonard, B.P., “The ULTIMATE Conservative Difference Scheme Applied to Unsteady One-Dimensional Advection,” Comput. Methods Appl. Mech. Eng., vol. 88, pp. 17-74, 1991.

34. Rubin, S.G. and Khosla, P.K., “Polynomial Interpolation Method for viscous Flow Calculations,” J. Comput. Phys., vol 27, pp. 153-168, 1982.

35. Rodi W., Majumdar S., Schonung B., Finite Volume Methods for Two-Dimensional Incompressible Flows with Complex Boundaries, Comp. Methods Appl. Mech. Eng., vol 75, pp. 369-392, 1989.

36. Gordon, W.J. and Thiel, L.C., ”Transfinite Mappings and Their Applications to Grid Generation,” in Thompson, J.F. (ed.), Numerical Grid Generation, North Holland, New York, pp. 171-192, 1982.

FIGURE CAPTIONS

Fig. 1 (a) Control Volume for HR interpolation; (b) Convective Boundedness Criterion on the Normalized Variable Diagram (NVD); (c) Control Volume for VHR streamline-based interpolation.

Fig. 2 Physical domain for pure convection of a scalar discontinuity.

Fig. 3 Comparison of ϕ-profiles along the vertical centerline of the domain for the pure convection of a scalar discontinuity problem using the HR and VHR schemes; (a) MINMOD; (b) OSHER; (c) MUSCL; (d) CLAM.

Fig. 4 Comparison of ϕ-profiles along the vertical centerline of the domain for the pure convection of a scalar discontinuity problem using the HR and VHR schemes; (a) SMART; (b) STOIC; (c) EXPONENTIAL; (d) SUPER-C.

Fig. 5 Physical domain, streamlines, boundary conditions, and dimensions for the sudden expansion of an oblique flow field in a rectangular cavity (Re=500).

Fig. 6 Comparison of the U-velocity profiles along the vertical centerline of the domain for sudden expansion of an oblique flow field in a rectangular cavity problem using the HR and VHR schemes; (a) MINMOD; (b) CLAM; (c) SMART; (d) STOIC.

Fig. 7 Comparison of the V-velocity profiles along the horizontal centerline of the domain `for sudden expansion of an oblique flow field in a rectangular cavity problem using the HR and VHR schemes; (a) MINMOD; (b) CLAM; (c) SMART; (d) STOIC.

Fig. 8 Physical domain and streamlines for the driven flow in a skew cavity problem (Re=500).

Fig. 9 Comparison of the U-velocity profiles along the vertical line X=0.85 for the driven flow in a skew cavity problem using the HR and VHR schemes; (a) MINMOD; (b) OSHER; (c) MUSCL; (d) CLAM.

Fig. 10 Comparison of the U-velocity profiles along the vertical line X=0.85 for the driven flow in a skew cavity problem using the HR and VHR schemes; (a) SMART; (b) STOIC; (c) EXPONENTIAL; (d) SUPER-C.

Fig. 11 (a) Physical domain and streamlines for gradual expansion in a non-orthogonal axi-symmetric channel; Comparison of the U-velocity profiles at X=6 using HR and VHR ((b) MINMOD, (c) SMART) schemes for test 4.

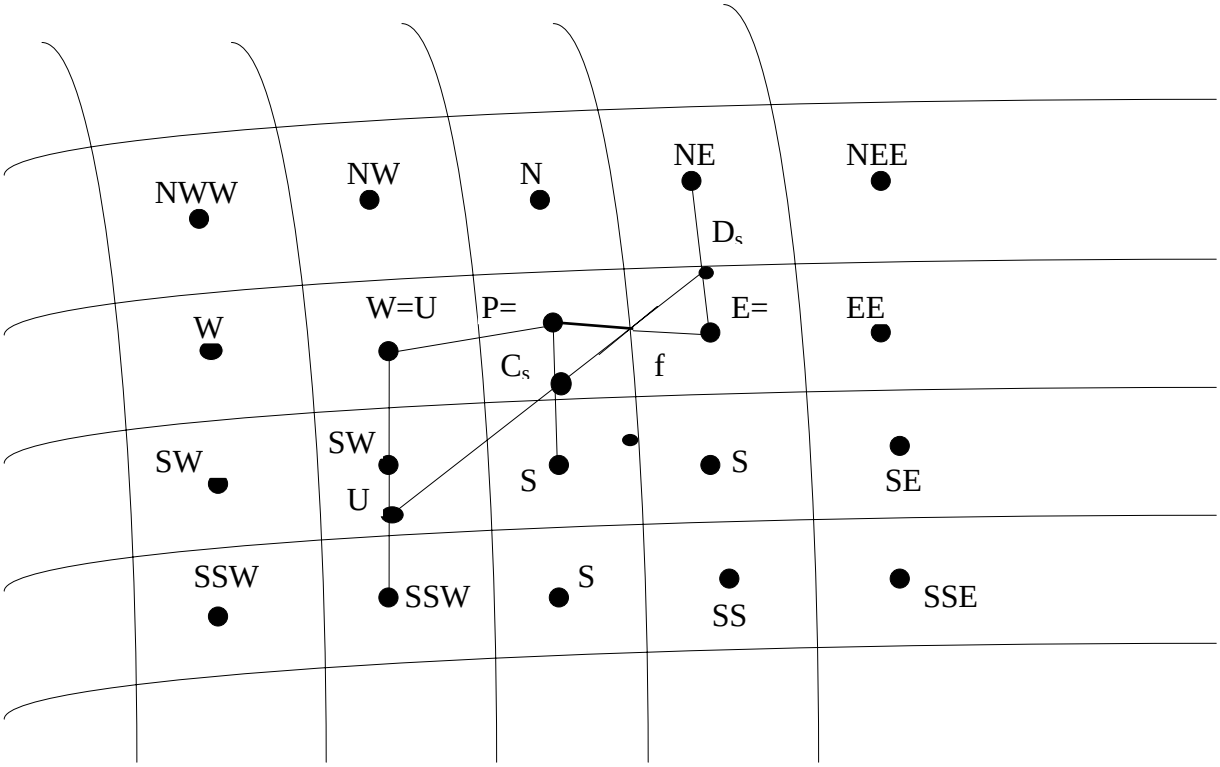

(a)

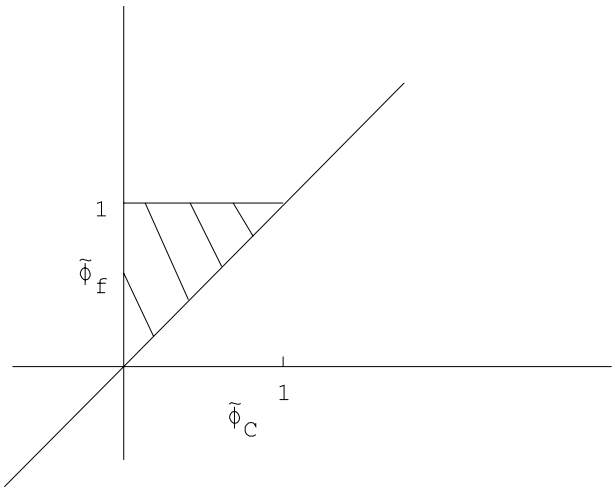

(b)

Fig. 1 (a) Typical grid point cluster, control volume, and streamline-based interpolation;

(b) Convective boundedness criterion on a Normalized Variable Diagram (NVD).

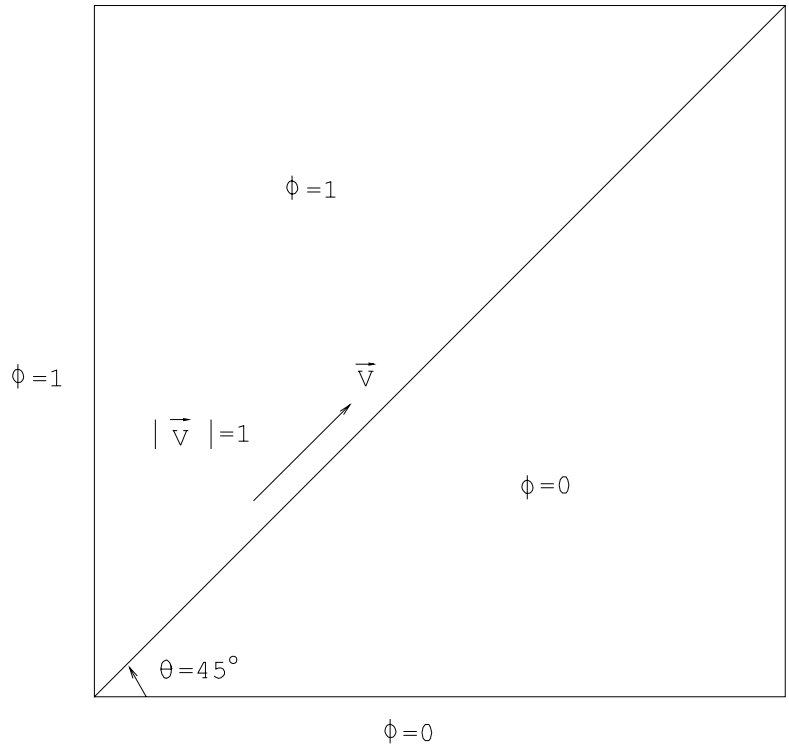

Fig. 2 Physical domain for pure convection of a scalar discontinuity.

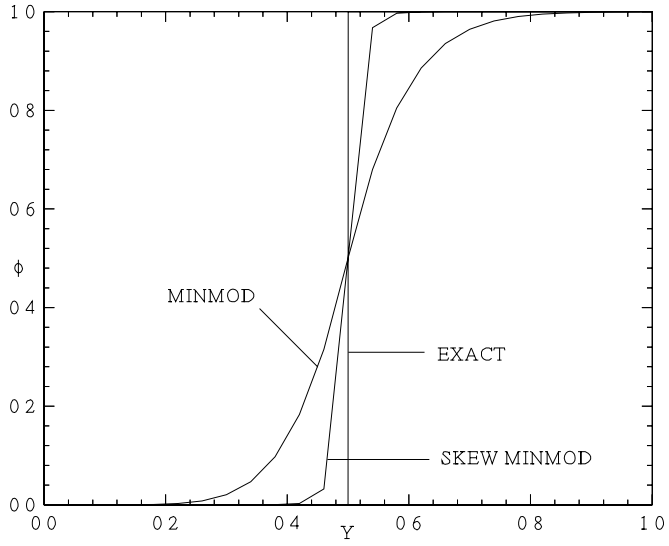
1 0
0 8
0 6
ϕ
0 4
0 2
0 0
0 0
0 2
0 4
Y
0 6
0 8
1 0
MINMOD
EXACT
SKEW MINMOD

(a)

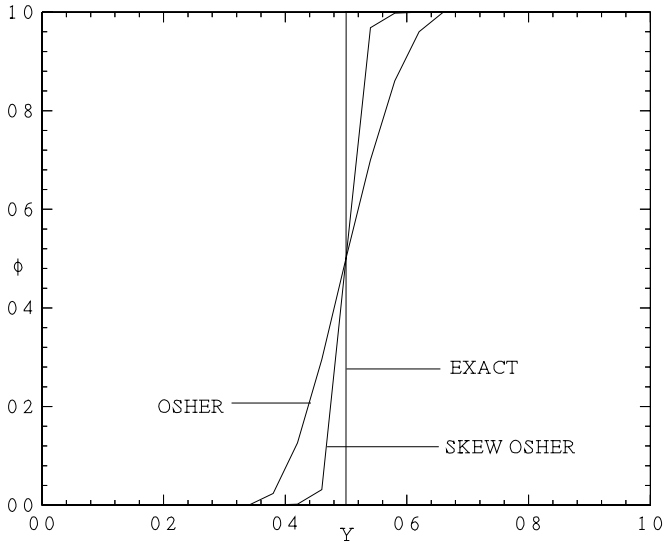
1 0
0 8
0 6
ϕ
0 4
0 2
0 0
0 0
0 2
0 4
Y
0 6
0 8
1 0
EXACT
OSHER
SKEW OSHER

(b)

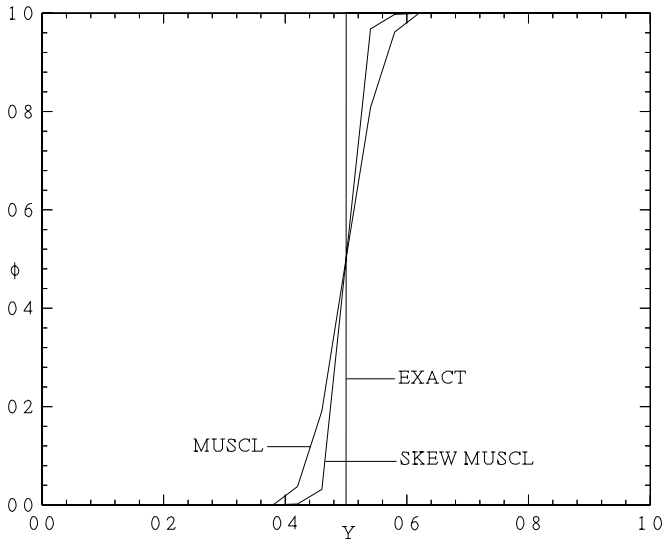

(c)

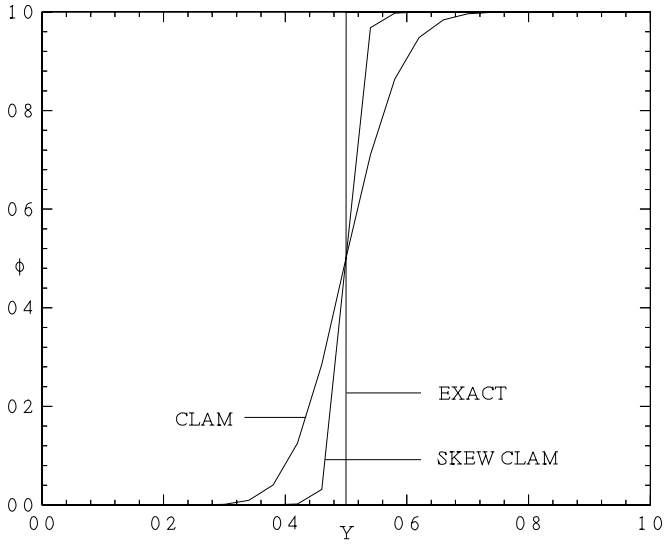

(d)

Fig. 3 Comparison of ϕ-profiles along the vertical centerline of the domain for the pure convection of a scalar discontinuity problem using the HR and VHR schemes; (a) MINMOD; (b) OSHER; (c) MUSCL; (d) CLAM.

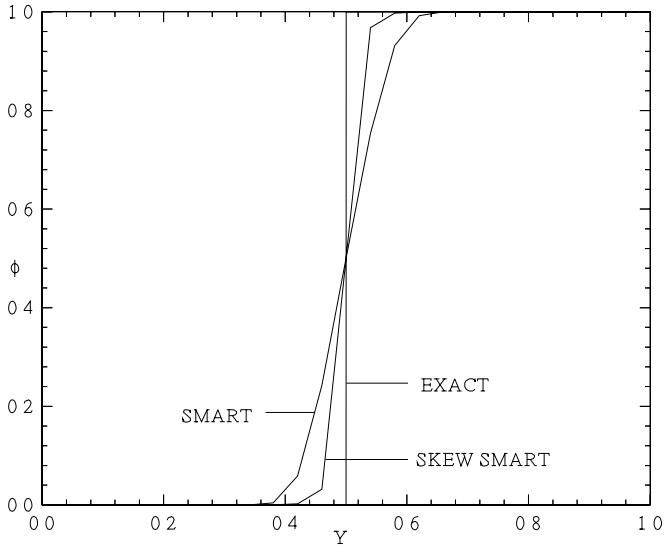
1 0
0 8
0 6
ϕ
0 4
0 2
0 0
0 0
0 2
0 4
0 6
0 8
1 0
Y
EXACT
SMART
SKEW SMART

(a)

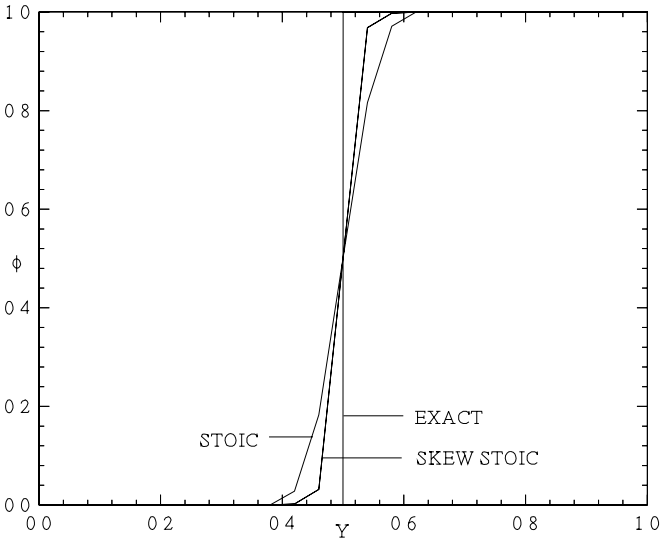
1 0
0 8
0 6
ϕ
0 4
0 2
0 0
0 0
0 2
0 4
0 6
0 8
1 0
Y
EXACT
STOIC
SKEW STOIC

(b)

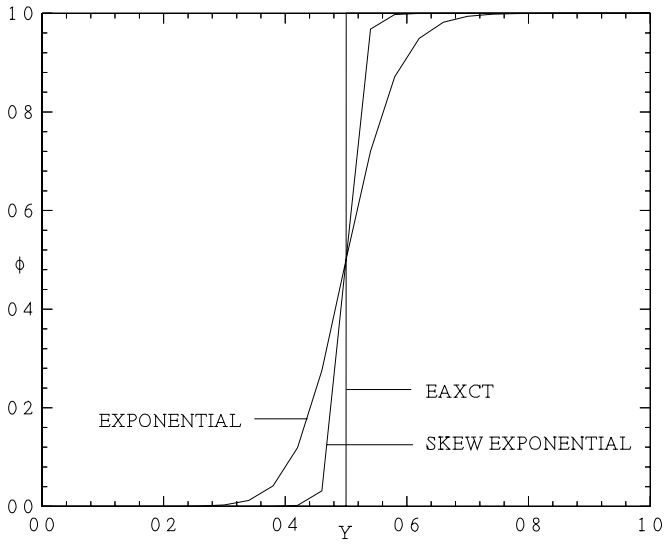

(c)

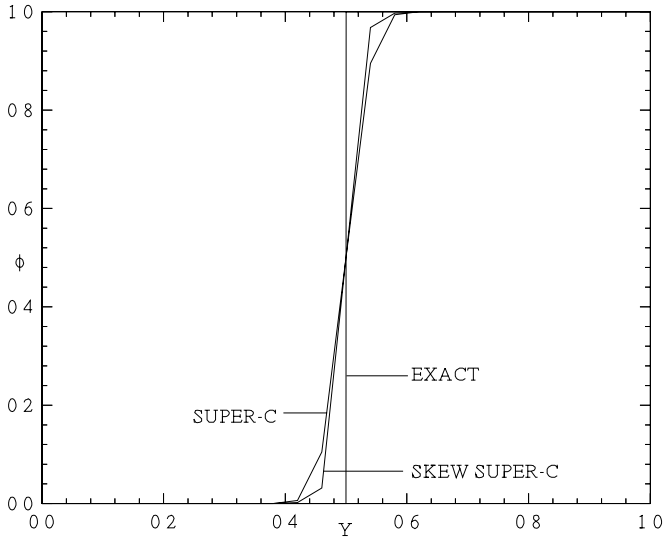

(d)

Fig. 4 Comparison of ϕ-profiles along the vertical centerline of the domain for the pure convection of a scalar discontinuity problem using the HR and VHR schemes; (a) SMART; (b) STOIC; (c) EXPONENTIAL; (d) SUPER-C.

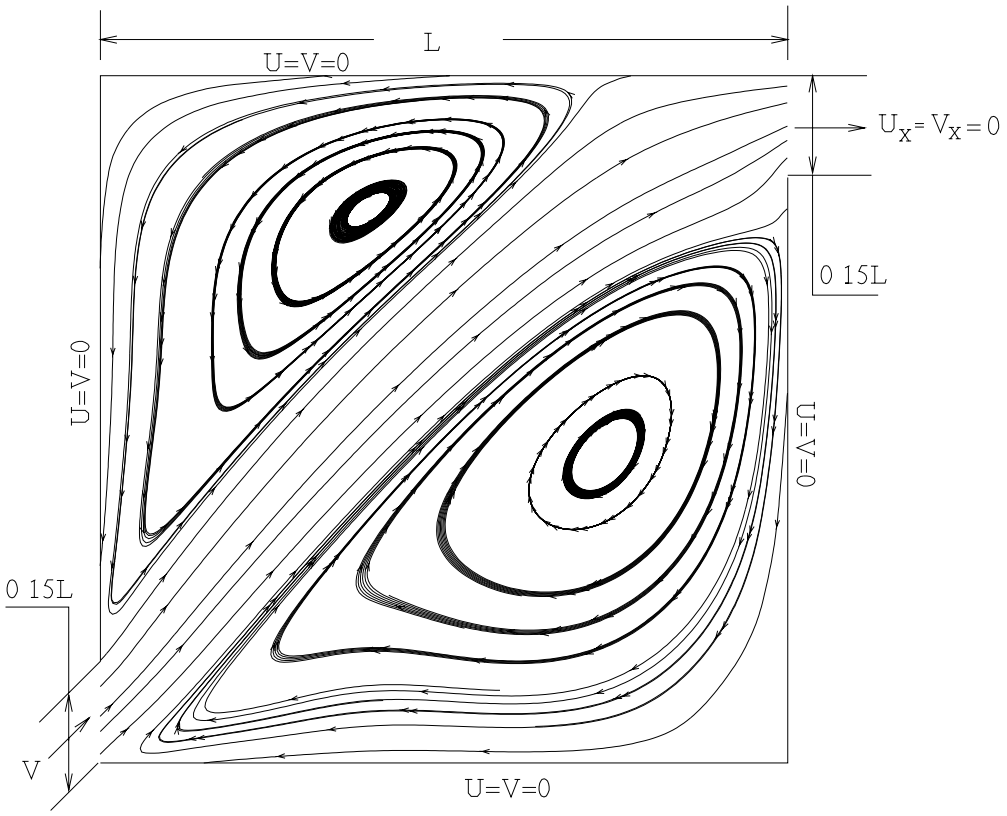

Fig. 5 Physical domain, streamlines, boundary conditions, and dimensions for the sudden expansion of an oblique flow field in a rectangular cavity (Re=500).

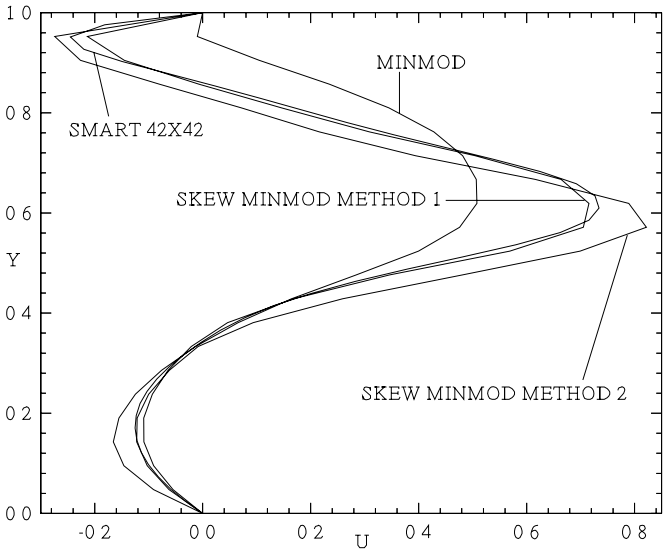
1 0
0 8
0 6
Y
0 4
0 2
0 0
-0 2
0 0
0 2
0 4
0 6
0 8
U
MINMOD
SMART 42X42
SKEW MINMOD METHOD 1
SKEW MINMOD METHOD 2

(a)

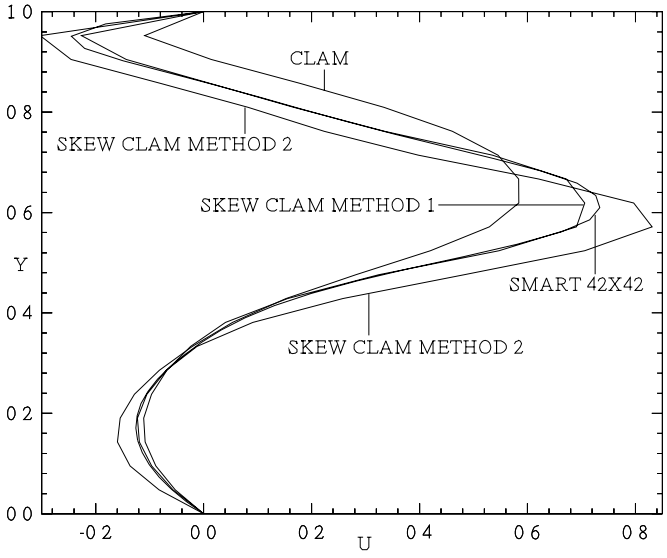
1 0
0 8
0 6
Y
0 4
0 2
0 0
-0 2
0 0
0 2
0 4
0 6
0 8
U
CLAM
SKEW CLAM METHOD 2
SKEW CLAM METHOD 1
SMART 42X42
SKEW CLAM METHOD 2

(b)

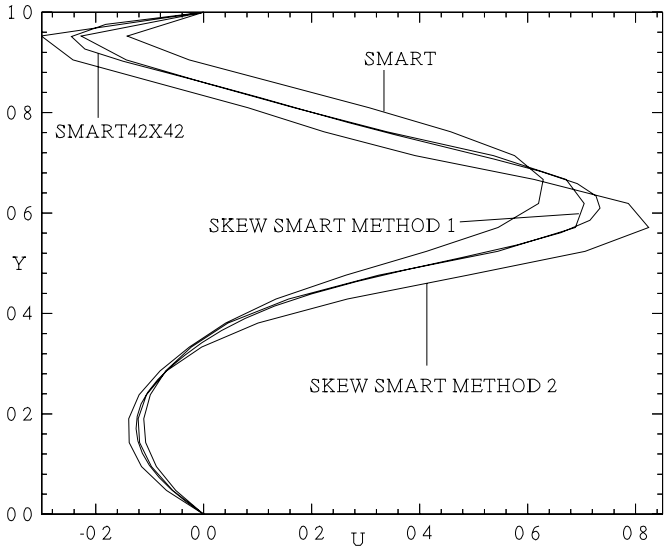

(c)

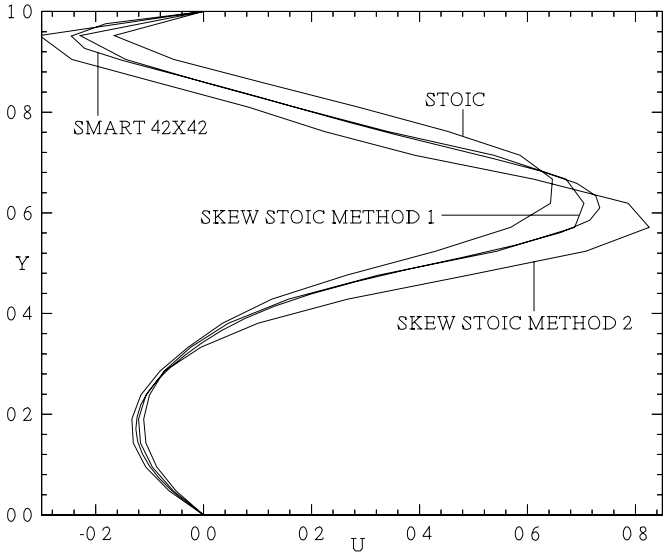

(d)

Fig. 6 Comparison of the U-velocity profiles along the vertical centerline of the domain for sudden expansion of an oblique flow field in a rectangular cavity problem using the HR and VHR schemes; (a) MINMOD; (b) CLAM; (c) SMART; (d) STOIC.

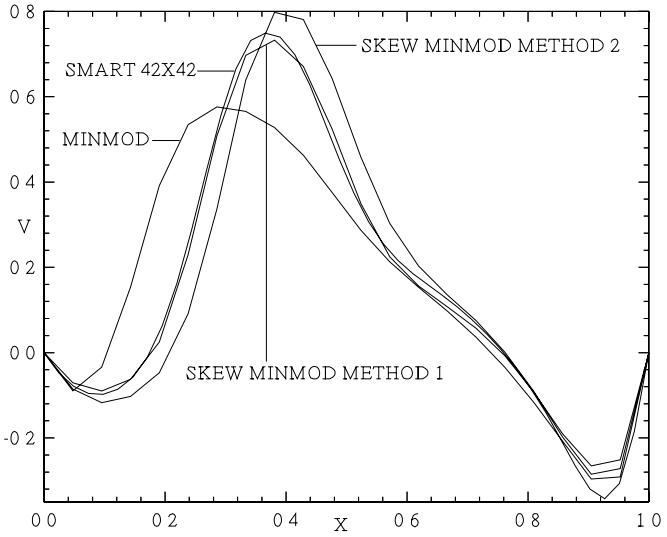
0 8
0 6
0 4
V
0 2
0 0
-0 2
SMART 42X42
MINMOD
SKEW MINMOD METHOD 2
SKEW MINMOD METHOD 1
0 0
0 2
0 4
X
0 6
0 8
1 0

(a)

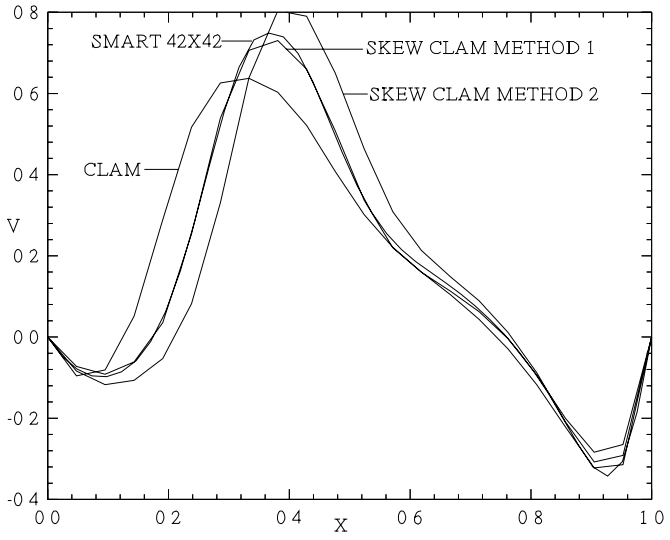
0 8
0 6
0 4
V
0 2
0 0
-0 2
-0 4
SMART 42X42
CLAM
SKEW CLAM METHOD 1
SKEW CLAM METHOD 2
0 0
0 2
0 4
X
0 6
0 8
1 0

(b)

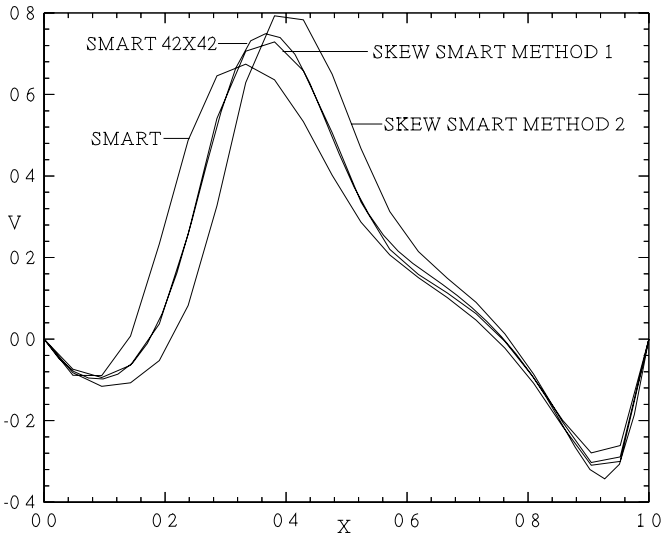

(c)

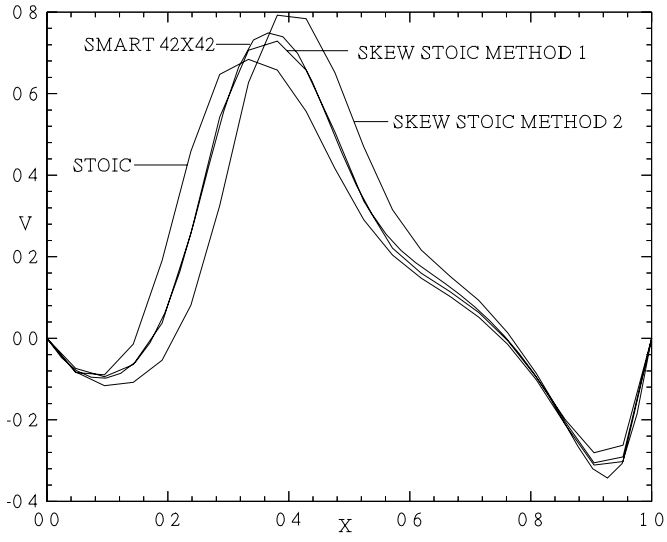

(d)

Fig. 7 Comparison of the V-velocity profiles along the horizontal centerline of the domain for sudden expansion of an oblique flow field in a rectangular cavity problem using the HR and VHR schemes; (a) MINMOD; (b) CLAM; (c) SMART; (d) STOIC.

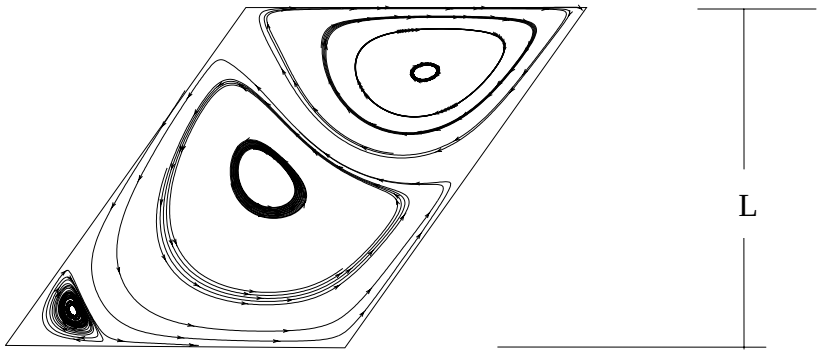

Fig. 8 Physical domain and streamlines for the driven flow in a skew cavity problem (Re=500).

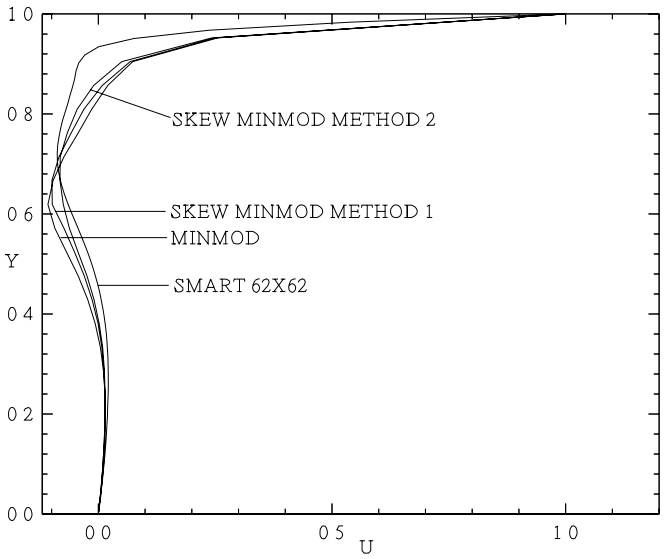
1 0
0 8
0 6
0 4
0 2
0 0
Y
0 0
0 5
1 0
U
SKEW MINMOD METHOD 2
SKEW MINMOD METHOD 1
MINMOD
SMART 62X62

(a)

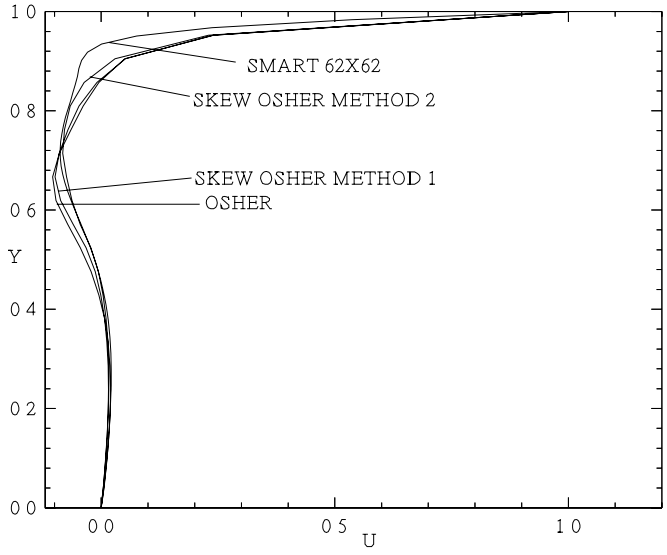
1 0
0 8
0 6
0 4
0 2
0 0
Y
0 0
0 5
1 0
U
SMART 62X62
SKEW OSHER METHOD 2
SKEW OSHER METHOD 1
OSHER

(b)

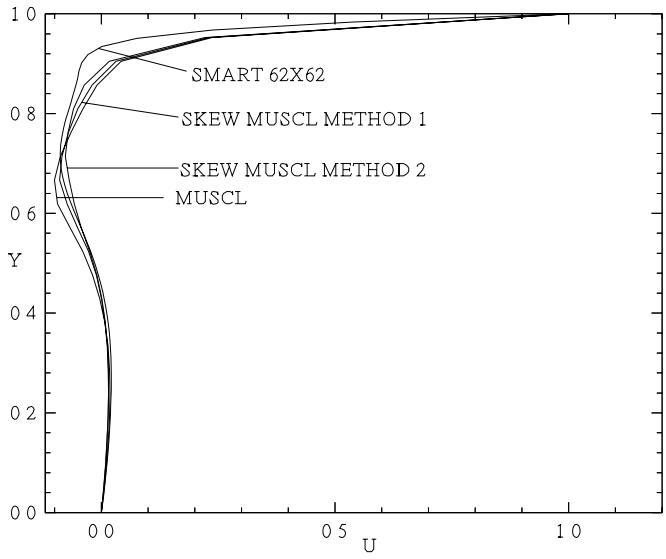

(c)

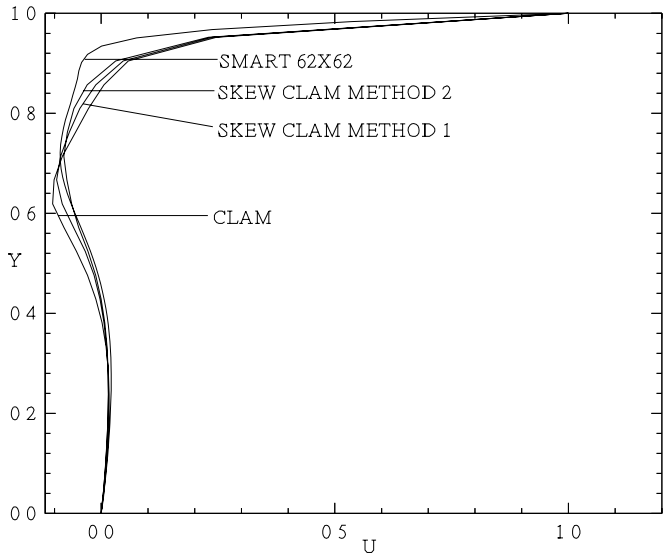

(d)

Fig. 9 Comparison of the U-velocity profiles along the vertical line X=0.85 for the driven flow in a skew cavity problem using the HR and VHR schemes; (a) MINMOD; (b) OSHER; (c) MUSCL; (d) CLAM.

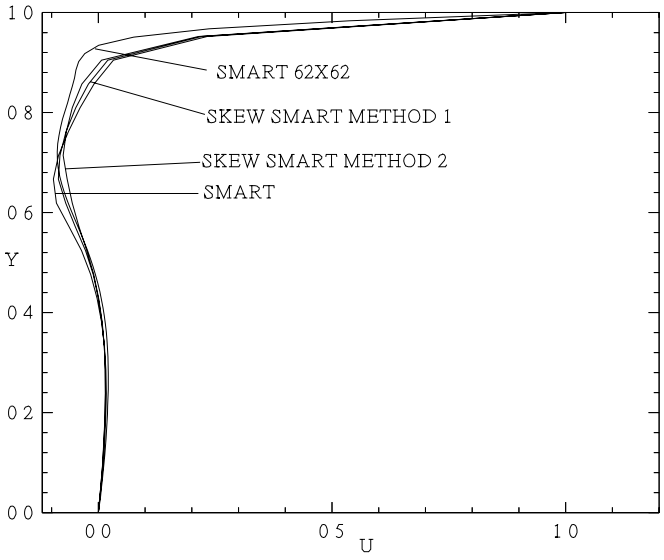
1 0
0 8
0 6
0 4
0 2
0 0
Y
0 0
0 5
1 0
U
SMART 62X62
SKEW SMART METHOD 1
SKEW SMART METHOD 2
SMART

(a)

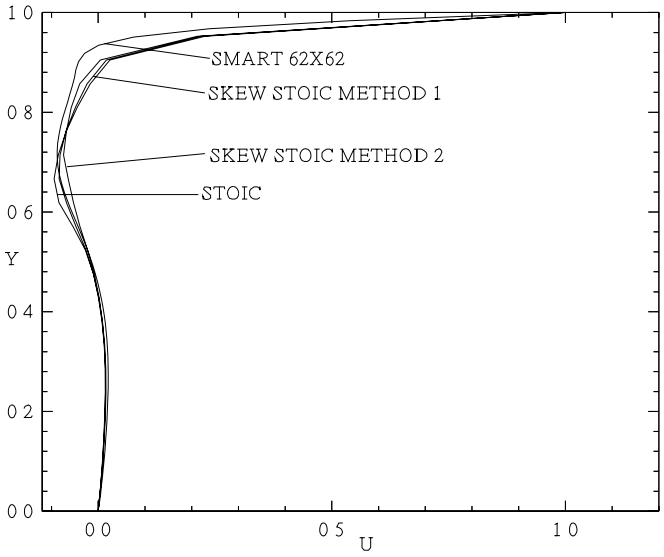
1 0
0 8
0 6
0 4
0 2
0 0
Y
0 0
0 5
1 0
U
SMART 62X62
SKEW STOIC METHOD 1
SKEW STOIC METHOD 2
STOIC

(b)

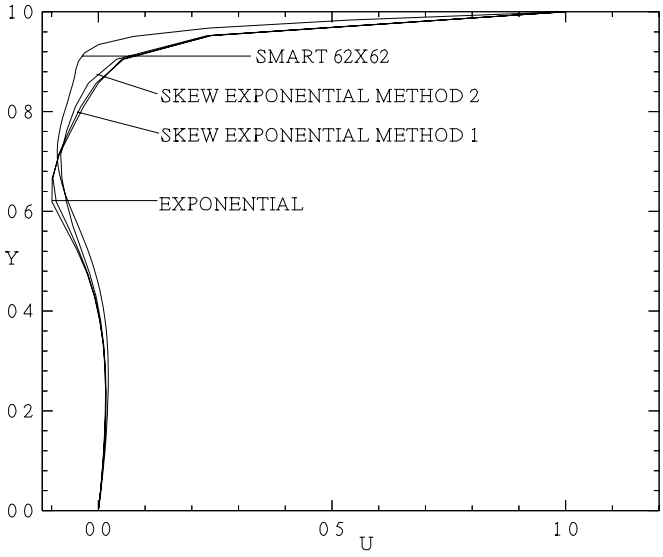

(c)

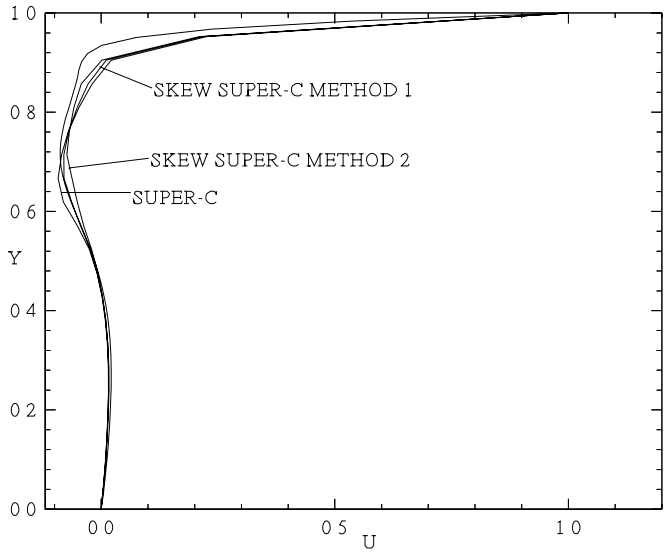

(d)

Fig. 10 Comparison of the U-velocity profiles along the vertical line X=0.85 for the driven flow in a skew cavity problem using the HR and VHR schemes; (a) SMART; (b) STOIC; (c) EXPONENTIAL; (d) SUPER-C.

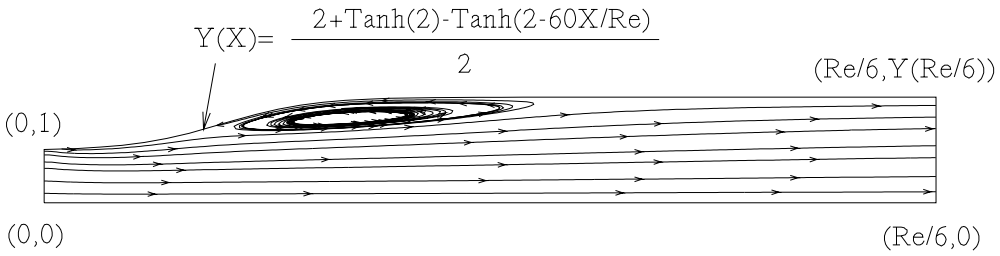

(a)

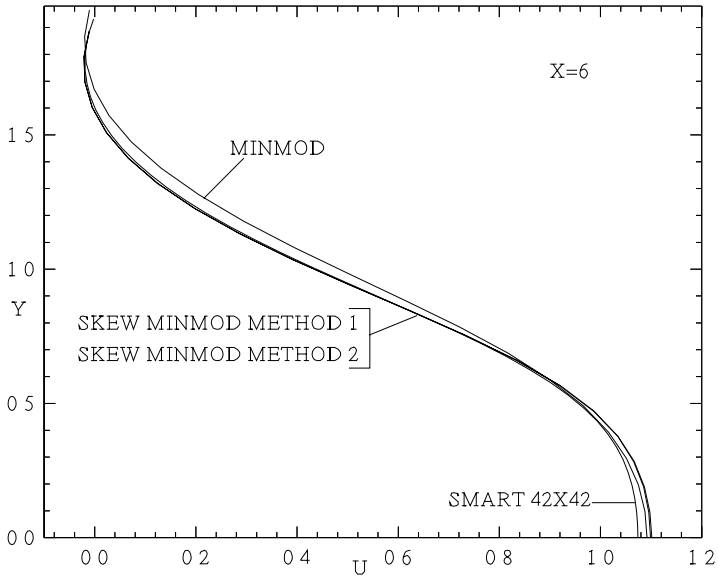

(b)

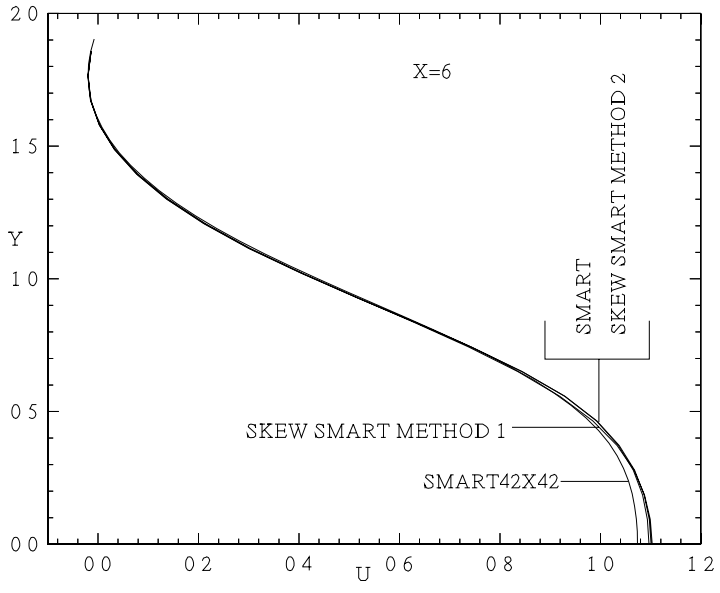

(c)

Fig. 11 (a) Physical domain and streamlines for gradual expansion in a non-orthogonal axi-symmetric channel; Comparison of the U-velocity profiles at X=6 using HR and VHR ((b) MINMOD, (c) SMART) schemes for test 4.